

Hydraulic Radius and Transport in Reconstructed Model Three-Dimensional Porous Media

DALE P. BENTZ and NICOS S. MARTYS

*Building and Fire Research Laboratory, Building 226 Room B-348,
National Institute of Standards and Technology, Gaithersburg, MD 20899, U.S.A.*

(Received: 5 October 1993; in final form: 20 April 1994)

Abstract. Methods for reconstructing three-dimensional porous media from two-dimensional cross sections are evaluated in terms of the transport properties of the reconstructed systems. Two-dimensional slices are selected at random from model three-dimensional microstructures, based on penetrable spheres, and processed to create a reconstructed representation of the original system. Permeability, conductivity, and a critical pore diameter are computed for the original and reconstructed microstructures to assess the validity of the reconstruction technique. A surface curvature algorithm is utilized to further modify the reconstructed systems by matching the hydraulic radius of the reconstructed three-dimensional system to that of the two-dimensional slice. While having only minor effects on conductivity, this modification significantly improves the agreement between permeabilities and critical diameters of the original and reconstructed systems for porosities in the range of 25–40%. For lower porosities, critical pore diameter is unaffected by the curvature modification so that little improvement between original and reconstructed permeabilities is obtained by matching hydraulic radii.

Key words: building technology, conductivity, critical diameter, hydraulic radius, permeability, porous media, reconstruction

1. Introduction

The efficiency of many technology processes such as filtration and catalysis and the durability of many materials such as concrete are highly dependent on the underlying transport properties of the relevant microstructure. Understanding the relationships between microstructure (or specifically pore structure) and transport is therefore critical for designing improved materials and systems. Computational materials science has advanced to the point where transport properties such as fluid permeability and electrical conductivity can be computed on quite large three-dimensional systems, containing as many as 256^3 nodes [1]. With the ever increasing processing speeds and memory capacities of computers, much larger systems will be tractable in the very near future. Now that these computational techniques have been developed, the bottleneck in elucidating microstructure-property relationships may be in obtaining adequate representations of the real three-dimensional microstructure of the porous media of interest.

Experimentally, three-dimensional images may be built up from a set of serial sections [2], but without the development of an automated system, this is a tedious

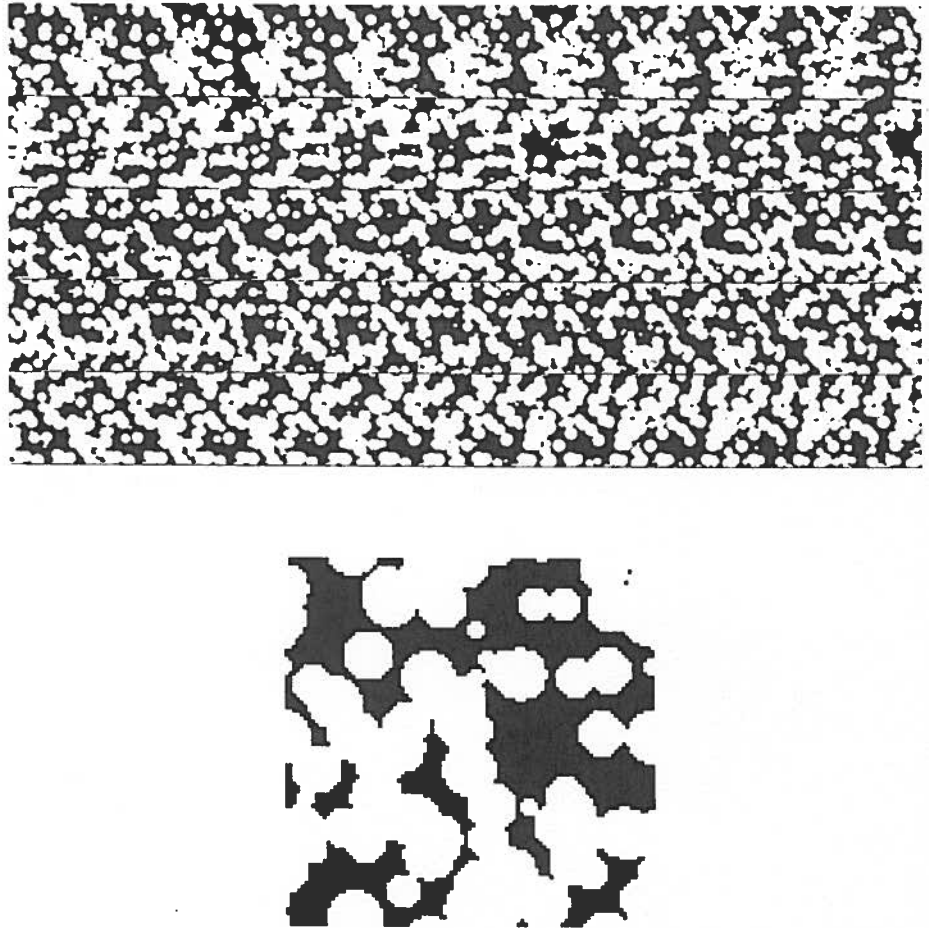


Fig. 1. Original 40% porosity microstructure showing (a) top 50 slices of 100^3 system (slices proceed from left to right; top to bottom) and (b) one of the slices selected for the reconstruction process.

and time-consuming task. X-ray microtomography offers one possibility for rapidly obtaining a three-dimensional image of a microstructure and resolution limits have improved to be on the order of several microns which may be adequate for many porous materials [3, 4]. Alternately, computer models may be used to generate three-dimensional microstructures of interest either by somewhat empirical rules as has been done for rocks [5] or by simulation of the underlying physical processes as has been done for cement paste [6]. While each of these models has proven extremely useful for a specific class of materials, their applicability to porous media in general is limited. The 'ideal' technique for creating three-dimensional porous media for computational analysis would be applicable to most porous media and would be based on a set of consistent procedures (or rules).

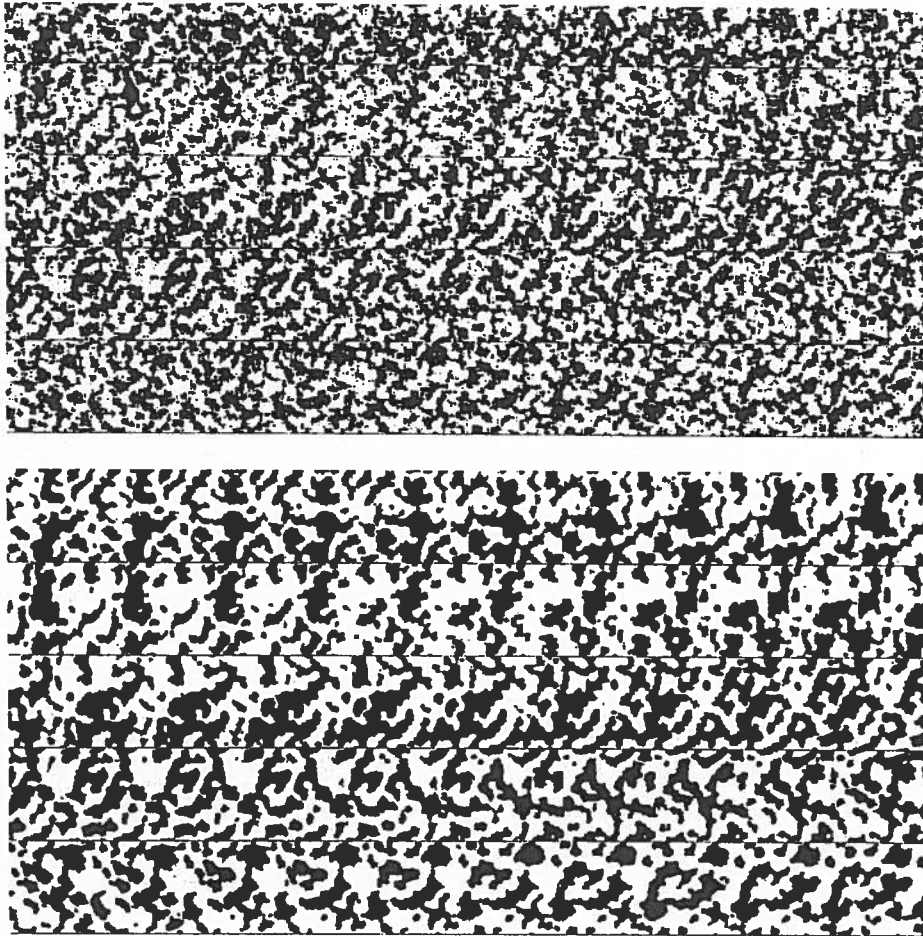


Fig. 2. Top 50 slices for (a) reconstructed and (b) modified three-dimensional microstructures for 40% porosity system.

In light of this, an attractive approach to this problem is to reconstruct a representative three-dimensional porous medium from a two-dimensional view of the system, such as that provided by a single micrograph illustrating the pore system. Based on the work of Joshi [7], Quiblier has developed a computational technique for creating a three-dimensional microstructure using autocorrelation analysis of a two-dimensional image [8]. Adler *et al.* [9] have utilized this technique to reconstruct Fontainebleau sandstones and have computed permeabilities [9] and conductivities [10] to compare to experimental measurements. Agreement was fair, but the transport properties (conductivity and permeability) of the reconstructed porous media were consistently lower than those of the real samples.

In this paper, a simplified version of the approach outlined by Quiblier and the effectiveness of a modification to the reconstructed microstructures based on

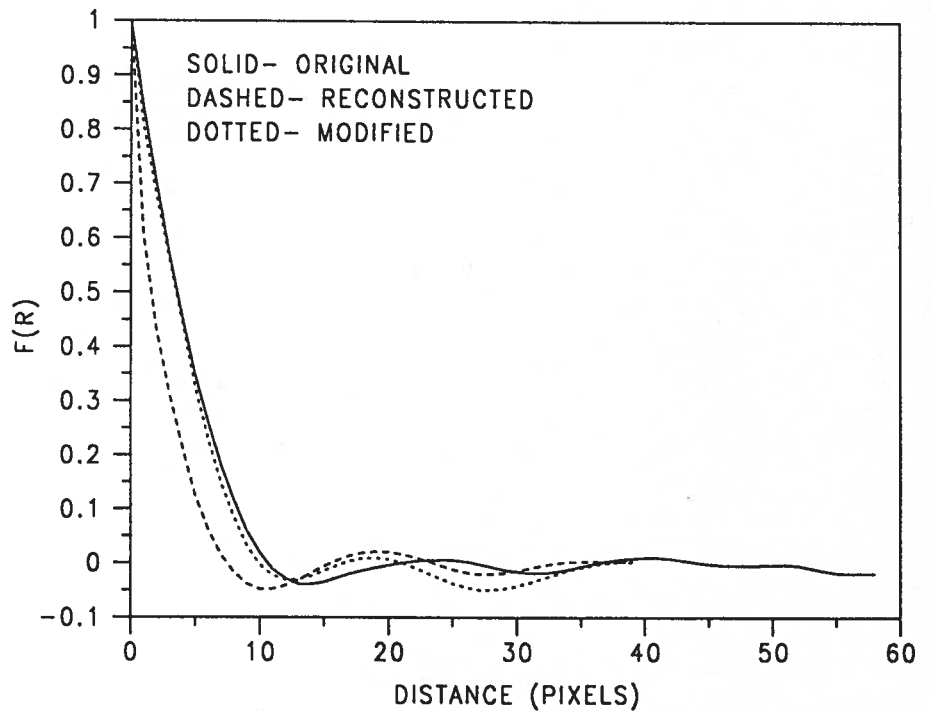


Fig. 3. Autocorrelation functions for original, reconstructed, and modified 40% porosity microstructures.

analysis of the hydraulic radius of the porous media are explored. Conductivities, permeabilities, and a critical pore diameter are all computed and used to evaluate the effectiveness of the reconstruction (original and modified) algorithms.

2. Computational Techniques

2.1. ORIGINAL MICROSTRUCTURE GENERATION

All of the techniques described in this paper are applied to digital-image based microstructures. Thus, in three dimensions, a microstructure consists of a three-dimensional grid (lattice) in which each site is defined to be either solid or pore. For the systems investigated here, the lattices were always $100 \times 100 \times 100$ units for a total of one million sites (pixels). To minimize finite size effects, periodic boundaries were utilized during microstructure generation. If a portion of a solid object, such as a sphere, extended outward through a face of the three-dimensional box, it was moved to the opposite face of the system.

To evaluate the reconstruction techniques employed in this paper, original microstructures based on a penetrable sphere model were selected. This model was selected because its correlation characteristics can be analytically determined [11] and its transport properties had been studied previously [1]. The microstructures

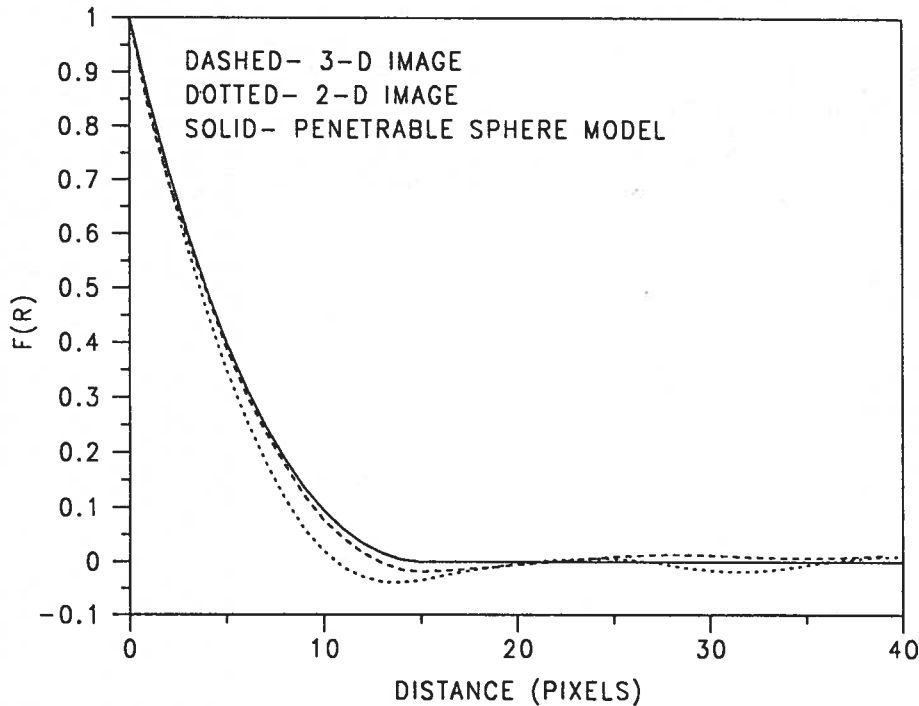


Fig. 4. Autocorrelation functions for two and three-dimensional images compared to analytical solution for penetrable spheres for 40% porosity microstructure.

were generated by centering solid digitized spheres at random locations (x, y, z) in the lattice using periodic boundary conditions. The spheres were allowed to freely overlap and porosities were varied between about 40 and 15% using two methods for lowering porosity. In method one, the initial system consisting of 500 spheres of diameter 15 pixels (lattice units) was modified by increasing the diameter of each sphere in increments of two up to a value of 19, without changing the centroids of the spheres. In the second method, the same initial system was modified by placing additional spheres into the system. Systems containing 500, 600, and 900 spheres were utilized. Thus, a total of five different original microstructures were generated and analyzed in this study.

2.2. TWO-DIMENSIONAL SLICE SELECTION AND THREE-DIMENSIONAL RECONSTRUCTION

For each of the original three-dimensional microstructures, five two-dimensional slices were selected at random locations in the z -plane. Each two-dimensional slice was used as a generating image in reconstructing a separate three-dimensional representation to be compared to the original three-dimensional microstructure.

The reconstruction technique employed for each two-dimensional image was as follows. First, the autocorrelation function for the image was computed. If the

two-dimensional image is defined as a discrete valued function, $I(x, y)$, where $I(x, y)$ is equal to one for solid pixels and zero for pore pixels, the two-point correlation function $S(x, y)$ for the image is given by [12]

$$S(x, y) = \sum_{i=1}^M \sum_{j=1}^N \frac{I(i, j) \times I(i+x, y+j)}{M \times N}, \quad (1)$$

where M and $N = 100$ for the images used here and periodic boundaries are used to define $I(i+x, j+y)$ when $(i+x, j+y)$ extends beyond the 100×100 two-dimensional image. $S(x, y)$ was determined for values of x and y ranging from 0 to 60 and was then converted to $S(r)$ for distances r in pixels by the equation [12]:

$$S(r) = \frac{1}{2r+1} \sum_{l=0}^{2r} S\left(r, \frac{\pi l}{4r}\right), \quad (2)$$

where $S(r, \theta) = S(r \cos \theta, r \sin \theta)$ was obtained by bilinear interpolation from the values of $S(x, y)$ determined above.

Similar to the approach used by Quiblier [8], the initial reconstructed three-dimensional image consisted of Gaussian distributed noise generated using a uniform random number generator [13] and the Box-Muller method [14] to convert the uniform random deviates to normal deviates. This three-dimensional noise image, $N(x, y, z)$ was directly filtered (or convolved) with the autocorrelation function, $F(x, y, z)$, defined as [15]

$$F(r) = F(x, y, z) = \frac{[S(r = \sqrt{x^2 + y^2 + z^2}) - S(0) \times S(0)]}{[S(0) - S(0) \times S(0)]}. \quad (3)$$

The resultant image, $R(x, y, z)$ was calculated as

$$R(x, y, z) = \sum_{i=0}^{30} \sum_{j=0}^{30} \sum_{k=0}^{30} N(x+i, y+j, z+k) \times F(i, j, k). \quad (4)$$

This is a simplification of the approach utilized by Quiblier [8], where a matrix of filtering coefficients is computed by solving a huge system of nonlinear equations. With this simplification, the autocorrelation function of the reconstructed porous medium will only approximate that of the original microstructure, and further modification may be required as outlined in section 2.3 below.

$R(x, y, z)$ was converted to a binary (0-pore or 1-solid) image by a thresholding operation. The threshold limits were determined by sampling all the values of $R(x, y, z)$ and computing a discrete histogram with 500 cells separating the minimum and maximum values of $R(x, y, z)$. This histogram was analyzed to determine the threshold value needed to match the porosity of the computed binary

image to that of the original three-dimensional image (not the two-dimensional slice). (The match is done against the porosity of the three-dimensional image as it is assumed that for a real material, the porosity could be assessed independently of the acquisition of a micrograph of the porous medium, via density determination, for example.) The porosity of the original three-dimensional microstructure was determined by simply counting the number of pixels in the $100 \times 100 \times 100$ system which were porosity. Based on this threshold value, a binary image exhibiting approximately the same porosity as the original three-dimensional microstructure was produced.

Finally, the three-dimensional autocorrelation function of the binary image was calculated for comparison to the autocorrelation function used in the filtering operation.

2.3. HYDRAULIC RADIUS MATCHING VIA SURFACE CURVATURE MODIFICATION

The final binary images from the image reconstruction process were further modified using an algorithm originally developed to simulate the sintering of ceramic powders [16, 17]. Here, the local surface curvature was determined at each pixel in the three-dimensional image by counting how many pore pixels are present in a sphere of some fixed diameter (typically seven pixels) centered at the pixel. Periodic boundary conditions were once again employed during this curvature computation. This measure has been shown to correspond directly to the local curvature [17]. After the curvatures were determined for all pixels, the binary image was modified by interchanging a fixed number (e.g., 200) of solid pixels of highest curvature with the same number of pore pixels of lowest curvature. All curvature values were then updated and the exchange process was repeated. Because the pore volume remains constant and the surface area decreases, this process has the effect of increasing the hydraulic radius (pore volume/surface area) of the microstructure. In every case investigated in this study, the hydraulic radius of the reconstructed binary image was less than that of the original generating structure. The surface curvature modification (exchange) algorithm was used to increase the hydraulic radius of the reconstructed image until it matched that of the two-dimensional generating image, which was somewhat different from the original three-dimensional microstructure due to sampling effects. The effects of this modification were evaluated qualitatively by viewing the original, reconstructed, and modified microstructures and quantitatively by evaluating their transport properties.

2.4. PERMEABILITY COMPUTATION

The permeability computation has been described in detail elsewhere [1, 18] but will be briefly outlined here. To compute permeability, the linear Stokes equations

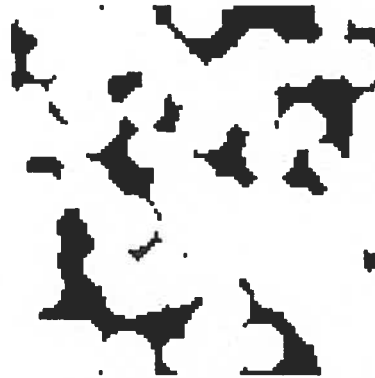
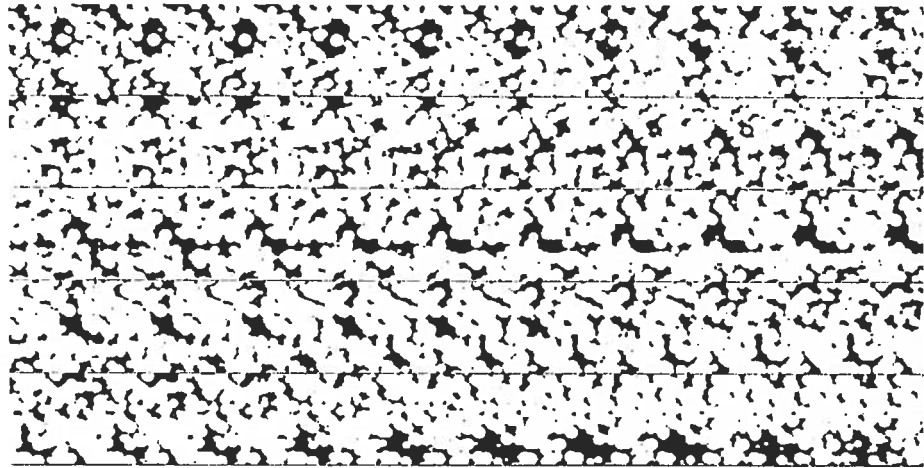


Fig. 5. Original 19% porosity microstructure showing (a) top 50 slices of 100^3 system (slices proceed from left to right; top to bottom) and (b) one of the slices selected for the reconstruction process.

are solved for the case of slow incompressible flow. These equations are of the form:

$$\eta \nabla^2 v(r) = \nabla p(r) \quad (5)$$

and

$$\nabla \cdot v(r) = 0 \quad (6)$$

where v and p are the local velocity and pressure fields respectively and η is the fluid viscosity. A pressure difference is prescribed across the three-dimensional microstructure and the above equations solved using a finite difference scheme in

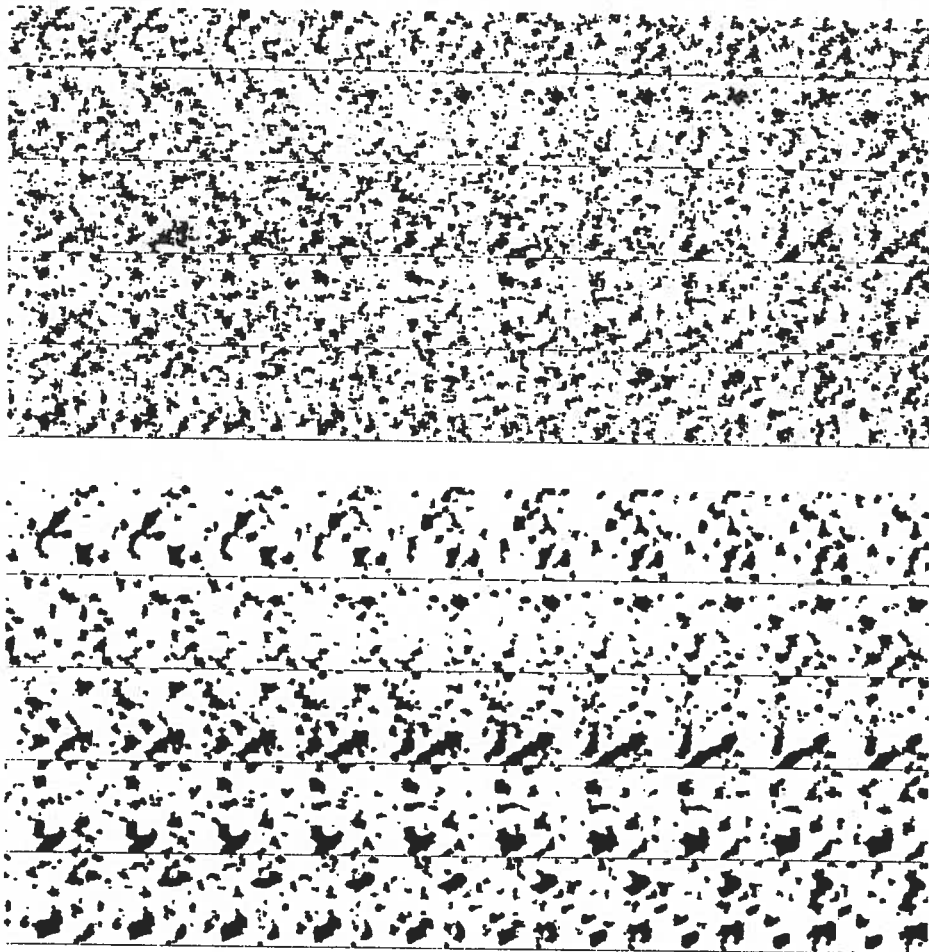


Fig. 6. Top 50 slices for (a) reconstructed and (b) modified three-dimensional microstructures for 19% porosity system.

conjunction with the artificial compressibility relaxation algorithm [18, 19]. The digital-image based microstructure is discretized into a marker-and-cell mesh [19] where pressures are defined at the lattice sites and fluid velocity components are defined along the center of bonds connecting sites. Near the solid-pore interfaces, non-centered difference equations are used to improve the accuracy of the solution and force the fluid velocities to zero at each interface. Once the system has sufficiently relaxed, the permeability, k , of the porous medium is calculated by volume averaging the local fluid velocity and applying the Darcy equation [20]

$$\langle v \rangle = -\frac{k \Delta P}{\eta L} \quad (7)$$

where L is the length of the sample (100 lattice units).

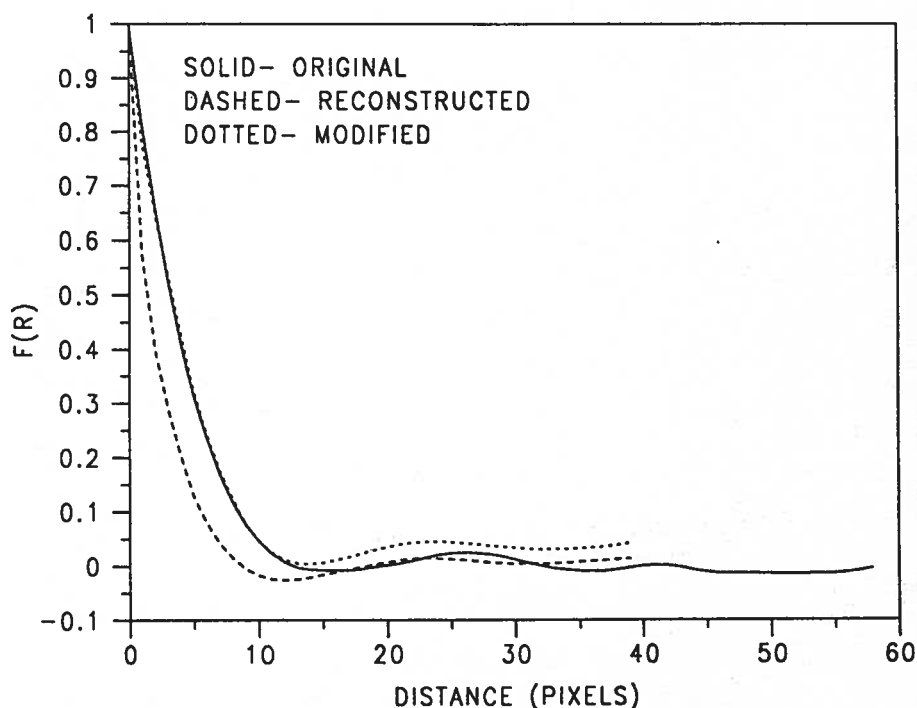


Fig. 7. Autocorrelation functions for original, reconstructed, and modified 19% porosity microstructures.

2.5. CONDUCTIVITY COMPUTATION

The conductivity calculation, basically a solution of the Laplace equation, has been described in detail elsewhere [18, 21] but will be briefly presented here. First, the three-dimensional microstructure is converted into a network of resistors by connecting each pair of adjacent pixels by a resistor. A resistor connecting two pore pixels is assigned a conductance of one while a resistor connecting two solid pixels or a pore and a solid pixel is assigned a conductance of zero. A voltage gradient is then applied across the sample and the system is relaxed using a conjugate gradient algorithm [22] to obtain the voltages at the nodes (center of each pixel). Knowing this voltage distribution allows one to calculate the total current and thus the equivalent relative conductivity, σ/σ_0 , for the microstructure. Here, σ is the conductivity of the porous medium and σ_0 is the conductivity of the solution in the pore space (taken to be one in these computations).

2.6. CRITICAL DIAMETER COMPUTATION

In addition to hydraulic radius, a critical diameter was computed as a characteristic length scale for each microstructure. The computation of this critical diameter is an extension of an algorithm to simulate mercury intrusion porosimetry in two

dimensions [23] and is equivalent to the concept of a critical sphere discussed by Thovert *et al.* [24].

Basically, the goal is to determine the size of the largest digitized sphere which can proceed (percolate) through the pore space from one side of the microstructure to the other. The test sphere is not allowed to overlap any solid regions of the microstructure. The diameter of the test sphere is increased from a value of three in increments of two pixel units. The critical diameter in pixel units is determined as the average of the largest diameter for which percolation occurs and the smallest diameter for which percolation doesn't occur. For cases where the smallest diameter for which percolation doesn't occur is three, a conventional burning algorithm [25] is used to assess the percolation of the pore space for a one-pixel diameter sphere. This length scale, commonly denoted D_c , has been shown, in combination with the relative conductivity, to be an excellent predictor of permeability for both model [1] and real porous media [26].

3. Results

3.1. IMAGES AND AUTOCORRELATION FUNCTIONS

Figure 1 shows the first 50 (out of 100) slices for the original 40% porosity microstructure along with a magnified view of one of the slices used as input into the reconstruction process. At this porosity, the pore structure appears relatively open even in two dimensions. Figure 2 shows the first 50 slices for the reconstructed and modified three-dimensional microstructures generated based on the two-dimensional slice in Figure 1b. The reconstructed system has some similarity to the original system but appears noisier with many isolated small solid areas breaking up larger porous regions. To the naked eye, the modified system appears much more similar to the original system than the reconstructed system does. This qualitative assessment is quantitatively verified in Figure 3 which shows the autocorrelation functions for all three systems. The original autocorrelation function was computed for the two-dimensional slice used to generate the reconstructed microstructure while the reconstructed and modified curves were computed for the entire new three-dimensional microstructures. The original and modified autocorrelation functions are seen to nearly overlap for values of distance up to 12 pixels. At longer lags, the functions no longer overlap as the reconstructed and modified systems are not able to match the long range order of the original microstructure. This could be due to the extent of the filtering operation used during the generation algorithm (30 pixels) or the random nature of the starting Gaussian noise image.

The autocorrelation function for the penetrable sphere model can be analytically determined as presented by Torquato and Stell [11]. Figure 4 shows a comparison of this analytical solution to the autocorrelation functions determined for a single two-dimensional slice and the overall three-dimensional microstructure for the 40% porosity system. For the three-dimensional image, minor variations between the analytical and computed autocorrelation function are observed. These are most

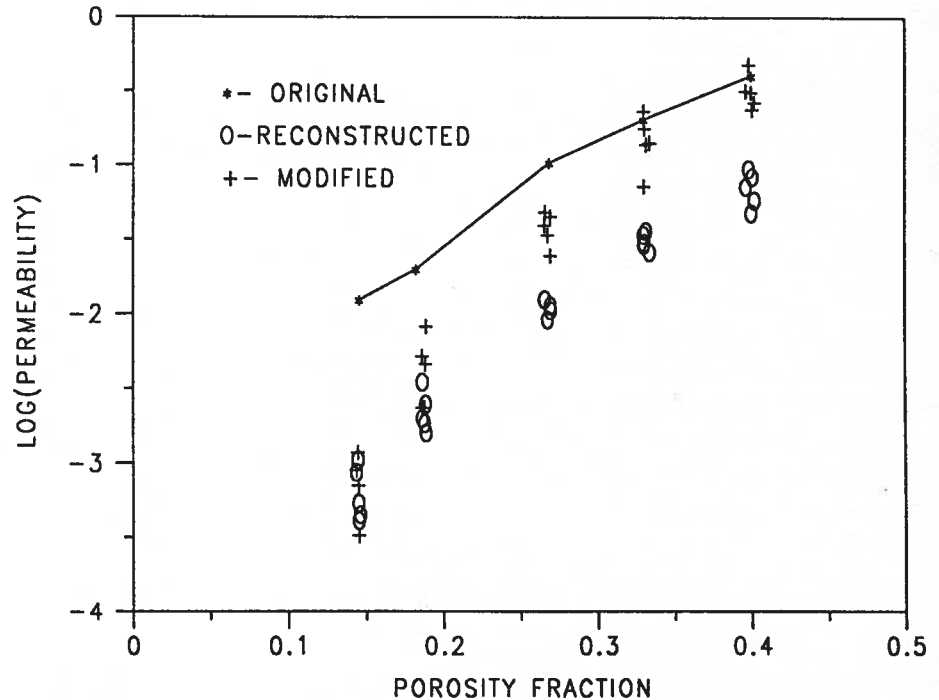


Fig. 8. Calculated permeabilities for original, reconstructed, and modified microstructures for five different porosities.

likely due to the fact that the model microstructure is a digitized image and the analytical solution is for a continuum microstructure. Indeed, similar effects of digitization on the autocorrelation functions of the penetrable-sphere model have been observed by Berryman [12]. For the two-dimensional image, the variation is somewhat larger since a single two-dimensional slice will have a different porosity and surface area than the overall three-dimensional system, due to statistical variation.

Results for a lower porosity (19%) system are presented in Figures 5–7. For this lower porosity system, the pore space is discontinuous in two dimensions although it remains percolated in three dimensions. Once again, the visual similarity between the modified and original microstructures is striking and the autocorrelation functions perfectly overlap one another for distances up to 10 pixels. In fact, the modified reconstruction algorithm appears to visually reproduce porous microstructures for the entire range of porosities (15–40%) investigated in this study.

3.2. CHARACTERISTIC LENGTH SCALES

Table I summarizes the results for the hydraulic radii and critical diameters measured for the original, reconstructed, and modified porous media. In general, the hydraulic radii of the reconstructed porous media were about half those of the

TABLE I. Characteristic length scales in pixel units for reconstructed porous media

| Porosity | D_c orig | D_c^a recon | D_c^a mod | R_h orig | R_h^a recon | R_h^a mod |
|----------|---------------|-----------------------|----------------|---------------|------------------|----------------|
| 0.400 | 8 | 4.0(0.0) ^b | 8.8(0.5) | 2.85 | 1.47(0.07) | 2.71(0.17) |
| 0.330 | 8 | 4.0(0.0) | 7.2(0.8) | 2.41 | 1.30(0.05) | 2.45(0.12) |
| 0.269 | 6 | 2.8(0.5) | 6.0(0.6) | 2.23 | 1.13(0.04) | 2.34(0.11) |
| 0.188 | 4 | 2.0(0.0) | 2.4(0.4) | 1.63 | 0.94(0.05) | 1.60(0.03) |
| 0.146 | 4 | 2.0(0.0) | 1.6(0.4) | 1.69 | 0.89(0.05) | 1.70(0.08) |

^a Average of five reconstructed/modified systems.

^b Numbers in parentheses indicate standard error for five reconstructed systems.

original microstructures. In Figure 2b, it appears that the curvature modification algorithm has opened the overall pore structure of the system. This is verified by the increase observed in the critical diameter between the reconstructed and modified porous media for porosities greater than 25%. For lower porosities, the critical diameter was not significantly affected by the curvature modification despite the increase in hydraulic radius. This may be due to the finite resolution of the 100^3 lattice used in this study, as at these very low values of D_c , the effects of the underlying pixel lattice structure are more pronounced.

3.3. TRANSPORT PROPERTIES

Figures 8 and 9 provide plots of permeability and relative conductivity, respectively, for the original, reconstructed, and modified porous media. The agreement between transport properties of the original and reconstructed microstructures is summarized in Table II. The curvature modification is seen to significantly improve the agreement between the permeabilities of the original and reconstructed microstructures for porosities greater than 25%. In fact, for porosities greater than 30%, the average values for the modified systems are within 25% of the actual values for the original microstructures. These are the same systems that exhibited a significant change in the critical diameter after curvature modification, suggesting that D_c is a more relevant characteristic length for permeability than R_h , at least for the systems investigated in this study.

In Figure 9, the curvature modification is seen to have very little effect on the relative conductivity of the reconstructed porous media. This suggests that the modification is changing the pore sizes much more than the overall tortuosity of the pore system. As shown in Table II, for porosities greater than 25%, however, the reconstructed and modified porous media exhibit relative conductivities within a factor of 2.5 of those of the original microstructures.

To adequately reconstruct a three-dimensional porous medium, it is vital to capture the three-dimensional percolation properties of the pore space as well as the

TABLE II. Average transport properties of reconstructed porous media

| Original Porosity | k (orig) pixels ² | k/k^* | k/k^* | (σ/σ_0) | $\frac{(\sigma/\sigma_0)}{(\sigma/\sigma_0)^*}$ | $\frac{(\sigma/\sigma)}{(\sigma/\sigma_0)^*}$ |
|-------------------|--------------------------------------|------------------------|----------------------|---------------------|---|---|
| | | $k^* = \text{Recon}^a$ | $k^* = \text{Mod}^a$ | | $^* = \text{Recon}^a$ | $^* = \text{Mod}^a$ |
| 0.400 | 0.41 | 5.7(0.27) ^b | 1.24(0.29) | 0.2 | 1.64(0.05) | 1.50(0.09) |
| 0.330 | 0.21 | 6.65(0.13) | 1.33(0.38) | 0.14 | 2.1(0.13) | 1.97(0.21) |
| 0.269 | 0.11 | 9.38(0.12) | 2.71(0.25) | 0.093 | 2.5(0.04) | 2.51(0.11) |
| 0.188 | 0.02 | 8.73(0.33) | 4.31(0.53) | 0.035 | 3.41(0.22) | 3.5(0.37) |
| 0.146 | 0.0125 | 18.94(0.43) | 19.84(0.75) | 0.026 | 7.22(0.22) | 10.6(0.58) |

^a Average of five reconstructed/modified systems.

^b Numbers in parentheses indicate coefficient or variation in k^* or $(\sigma/\sigma_0)^*$ for the 5 reconstructed systems.

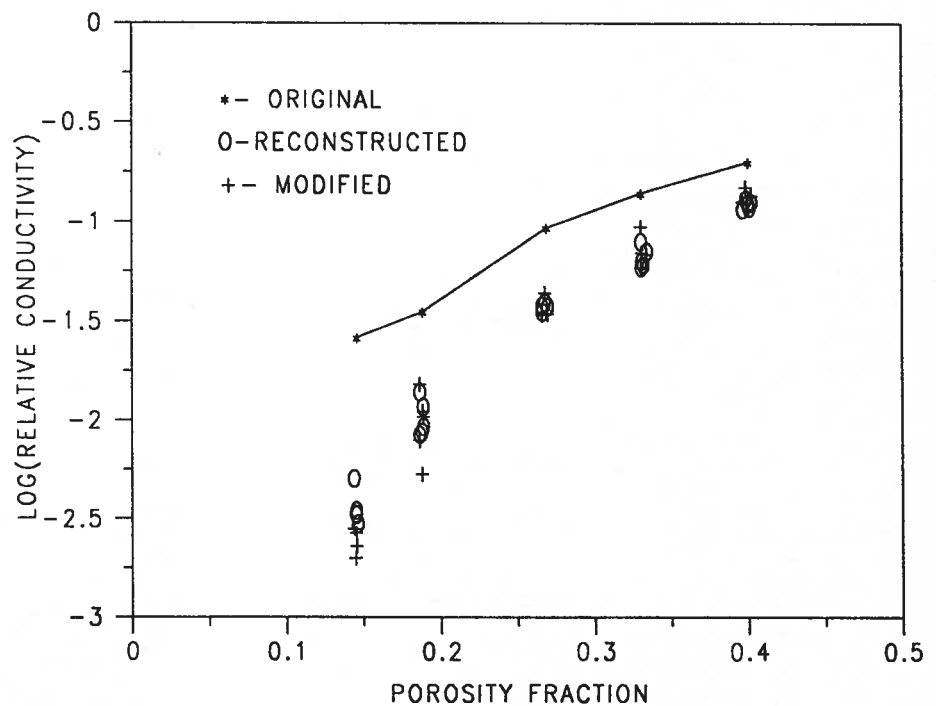


Fig. 9. Calculated relative conductivities for original, reconstructed, and modified microstructures for five different porosities.

two-dimensional characteristics of the pores. Since the starting point in this study is a two-dimensional image of the pore system, capturing the three-dimensional connectivity is indeed the research challenge. For the penetrable sphere model, it is well known that the pore (matrix) phase has a percolation threshold of about

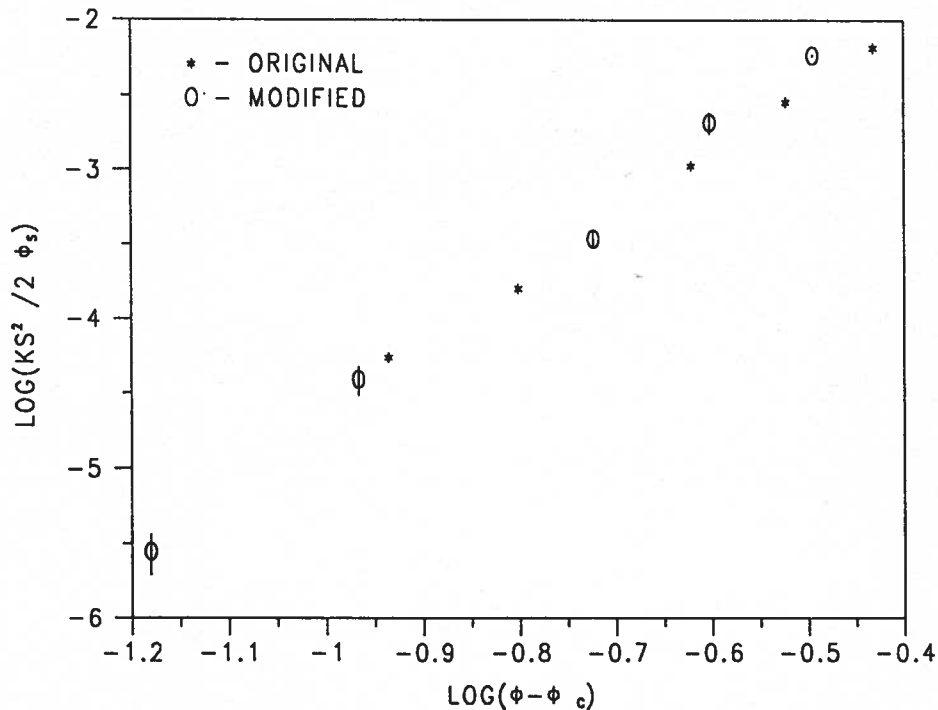


Fig. 10. Scaled permeabilities for original and modified reconstructed microstructures for five different porosities. Vertical bars for modified systems indicate standard error in computed scaled permeabilities.

3% [27]. From our studies, the reconstructed microstructures appear to exhibit a percolation threshold closer to 10% porosity. This difference in connectivity between original and reconstructed microstructures was alluded to by Adler *et al.* [9] as one of the main reasons for differences between the transport properties of the two types of media. In this study, while good agreement has been obtained between transport properties for porosities far away from the apparent percolation thresholds of the model and reconstructed media (i.e. > 25%), large differences have been observed in values for porosities nearer to these percolation thresholds (i.e. < 20%).

The percolation threshold of about 10% observed for the reconstructed systems may be an inherent limitation of the reconstruction technique employed in this study, as a similar threshold has been obtained for systems based on thresholding three-dimensional images of Gaussian-filtered white noise [5]. Furthermore, Renault [28] has observed a reduction in the percolation threshold for site percolation on a three-dimensional network from a value of 0.31 to a value between 0.1 and 0.2 when a variety of different spatial correlations were introduced. To obtain a significantly lower percolation threshold, it may be necessary to utilize higher order information such as a three-point correlation function or start with

a different initial three-dimensional image structure than the image of Gaussian noise employed in this study.

Martys *et al.* [29] have developed a universal scaling relationship for the permeability of a porous medium as a function of its porosity and percolation threshold. The basic equation is of the form

$$\frac{ks^2}{2\phi_s} \alpha (\phi - \phi_c)^n \quad (8)$$

where s is the specific surface of the porous medium, ϕ_s is the solids fraction, ϕ is the porosity, ϕ_c is the percolation threshold for porosity, and n is a critical exponent. Figure 10 provides a plot of this universal scaling for values of ϕ_c of 0.03 and 0.08 for the original and modified reconstructed porous media respectively. A value of 0.08 was selected as the percolation threshold for porosity in the reconstructed media on the basis that the porosity was connected for reconstructed systems with 10.5% porosity but disconnected for systems with 7.2% porosity. In figure 10, all the data points are seen to lie on a single line, with some scatter, further confirming that the differences in permeability between the original and modified systems are largely due to their different percolation thresholds.

4. Conclusions

A modified reconstruction algorithm has been presented for generating a three-dimensional microstructure from a single two-dimensional image of an isotropic porous medium based on overlapping spheres. For these model systems, the algorithm was observed to reproduce visual characteristics of the original systems for porosities ranging from 15–40%. The reconstruction algorithms have also been evaluated based on their ability to reproduce the transport properties of the original systems. For porosities greater than 25%, both the average relative conductivity and permeability of the modified systems were within a factor of 2.7 of the values for the original system. For porosities greater than 30%, the average permeabilities of the modified systems were within 25% of the permeabilities of the original microstructures. These improvements in permeability agreement have been related to the critical diameter measure for the microstructures. For lower porosity (< 20%) systems, the modification algorithm had little effect on this critical diameter and thus little improvement was observed in the permeability values of the modified reconstructed systems. All reconstructed systems appear to exhibit a pore space percolation threshold of 8%, significantly higher than the 3% value for the original penetrable sphere system, which further contributes to the disagreement in transport properties for the lower porosity systems.

Acknowledgements

The authors would like to thank Kevin Coakley of the NIST Statistical Engineering Division and Ed Garboczi and Ken Snyder of the NIST Building Materials Division for useful discussions.

References

1. Schwartz, L. M., Martys, N., Bentz, D. P., Garboczi, E. J., and Torquato, S.: Cross property relations and permeability estimation in model porous media, *Phys. Rev. E* **48**(6) (1993), 4584–4591.
2. Stutzman, P. E.: Serial sectioning of hardened cement paste for scanning electron microscopy, *Ceramic Trans.* **16**, (1991), 237.
3. Schwartz, L. M., Auzeais, F., Dunsmuir, J., Martys, N., Bentz, D. P., and Torquato, S.: Transport and diffusion in three-dimensional composite media, *Physica A: Proc. Third Internat. Meeting on Electrical Transport and Optical Properties of Inhomogeneous Media (ETOPIM3)* **207**, (1994), 28–36.
4. Flannery, B. P., Deckman, H. W., Roberge, W. G., and D'Amico, K. L.: Three-dimensional X-ray microtomography, *Science* **237**, (1987), 1439–1444.
5. Crossley, P. A., Schwartz, L. M., and Banavar, J. R.: Image-based models of porous media: Application of Vycor glass and carbonate rocks, *Appl. Phys. Lett.*, **59**(27), (1991), 3553–3555.
6. Bentz, D. P. and Garboczi, E. J.: Percolation of phases in a three-dimensional cement paste microstructural model, *Cement Concrete Res.* **21**(2), (1991), 325–344.
7. Joshi, M.: A class of stochastic models for porous media, Ph. D. Thesis, Univ. of Kansas, 1974.
8. Quiblier, J. A.: A new three-dimensional modeling technique for studying porous media, *J. Colloid Interface Sci* **98**(1), (1984), 84–102.
9. Adler, P. M., Jacquin, C. G., and Quiblier, J. A.: Flow in simulated porous media, *Internat. J. Multiphase Flow* **16**(4), (1990), 691–712.
10. Adler, P. M., Jacquin, C. G., and Thovert, J. F.: The formulation factor of reconstructed porous media. *Water Resour. Res.* **28**(6), (1992), 1571–1576.
11. Torquato, S. and Stell, G.: Microstructure of two-phase random media. III. The n -point matrix probability functions for fully penetrable spheres, *J. Chem. Phys.* **79**(3), (1983), 1505–1510.
12. Berryman, J. G.: Measurement of spatial correlations functions using image processing techniques, *J. Appl. Phys.* **57**(7), (1985), 2374–2384.
13. Press, W. H. and Teukolsky, S. A.: *Comput. Phys.* **6**(5), (1992), 522–524.
14. Law, A. M. and Kelton, W. D.: *Simulation Modeling and Analysis*, McGraw-Hill, New York, (1982), Chap. 7.
15. Cressie, N.: *Statistics for Spatial Data*, Wiley, New York, (1991), Chap. 2.
16. Bentz, D. P., Garboczi, E. J., Pimentia, P. J. P., and Carter, W. C.: Cellular automaton simulations of surface mass transport due to curvature gradients: Simulation of sintering, in *Synthesis and Processing of Ceramics: Scientific Issues*, MRS Proceedings, Vol, 249, (1992), 413–418 pp.
17. Pimentia, P. J. P., Carter, W. C., and Garboczi, E. J.: Cellular automaton algorithm for surface mass transport due to curvature gradients: Simulations of sintering, *Comp. Mat. Sci.* **1**, (1992), 63–77.
18. Martys, N. and Garboczi, E. J.: Length scales relating the fluid permeability and electrical conductivity in random two-dimensional model porous media, *Phys. Rev. B* **46**, (1992), 6080.
19. Peyret, R. and Taylor, T. D.: *Computational Methods for Fluid Flow* Springer-Verlag, New York, 1983.
20. Adler, P. M.: *Porous Media: Geometry and Transports*, Butterworth-Heinemann, Boston, 1992.
21. Garboczi, E. J. and Bentz, D. P.: Computer simulation of the diffusivity of cement-based materials, *J. Mat. Sci.* **27**, (1992), 2083–2092.
22. Press, W. H., Flannery B. P., Teukolsky, S. A. and Vetterling, W. T.: *Numerical Recipes: The Art of Scientific Computing*, Cambridge University Press, Cambridge, 1986, Chap. 10.

23. Garboczi, E. J. and Bentz, D. P.: Digitized simulation of Mercury intrusion porosimetry, *Ceramic Trans.* **16** (1991), 365.
24. Thovert, J. F., Salles, J., and Adler, P. M.: Computerized characterization of the geometry of real porous media: Their discretization, analysis, and interpretation, *J. Microscopy* **170**(1), (1993), 65-79.
25. Stauffer, D.: *Introduction of Percolation Theory*, Taylor and Francis, London, 1985.
26. Katz, A. J. and Thompson, A. H.: *Phys. Rev. B.* **34**, 8179, 1986; *J. Geophys. Res.* **92**, (1987), 599.
27. Elam, W. T., Kerstein, A. R., and Rehr, J. J.: Critical properties of the void percolation problem for spheres, *Phys. Rev. Lett.* **52**(17), (1984), 1516-1519.
28. Renault, P.: The effect of spatially correlated blocking-up of some bonds or nodes of a network on the percolation threshold, *Transport in Porous Media* **6**, (1991), 451-468.
29. Martys, N. S., Torquato, S. A., and Bentz, D. P.: Universal scaling of fluid permeability for sphere packings, *Phys. Rev. E* **50**(1), (1994), 403-408.